Technical Report

TR-99-25

Representation of fracture networks as grid cell conductivities

Urban Svensson
Computer-aided Fluid Engineering AB

December 1999

SKB

Representation of fracture networks as grid cell conductivities

Urban Svensson

Computer-aided Fluid Engineering AB

December 1999

ABSTRACT

A method to represent fracture networks as grid cell conductivities is described and evaluated. The method is developed for a fracture system of the kind found in the Äspö area, i.e. a sparsely fractured rock with a conductivity field that is dominated by a set of major fracture zones. For such a fracture system it is believed that an accurate description of the correlation and anisotropy structure is essential. The proposed method will capture these features of the fracture system.

The method will be described in two reports. The first one, this report, evaluates the accuracy by comparisons with analytical solutions and established theories. The second report is an application to the Äspö Hard Rock Laboratory.

The general conclusion from this report is that the method is accurate enough for practical groundwater simulations. This statement is based on the results from three testcases with analytical solution and two testcases where results are compared with those from established theories.

ABSTRACT (Swedish)

En metod för att representera spricknätverk som cellkonduktiviteter i en kontinuummodell presenteras och utvärderas. Metoden utgår från ett spricksystem av den typ som återfinns i Äspö-området, dvs ett system där ett fåtal sprickzoner antas dominera konduktivitetsfältet. För sådana system bör det vara väsentligt att beskriva konduktivitetsfältets anisotropi och korrelationsstruktur på ett korrekt sätt. Den föreslagna metoden avser att beskriva dessa egenskaper hos konduktivitetsfältet.

Metoden beskrivs i två rapporter, varav denna är den första. Syftet med denna rapport är att utvärdera metodens noggrannhet genom jämförelser med analytiska lösningar och resultat från etablerade teorier. I rapport nummer två beskrivs en tillämpning på Äspö-området.

Den allmänna slutsatsen från rapporten är att metoden är tillräckligt noggrann för simuleringar av naturligt förekommande grundvattensystem. Denna slutsats baseras på resultaten från tre testfall med analytisk lösning och två fall där kvalitativa jämförelser med etablerade teorier genomförs.

TABLE OF CONTENTS

1 INTRODUCTION

Most numerical models of groundwater flows subdivides the studied domain into smaller volumes. If a computational grid is defined we call these smaller volumes grid cells and we apply the conservation laws and other constitutive relations to these. Also material properties, like hydraulic conductivity and porosity, need to be specified for the grid cells. These properties are often measured on a smaller scale (support scale) and a technique to express these on the scale of the grid cells is thus needed (upscaling). When material properties for all grid cells have been obtained, the flow simulation can be performed. In this report we will however not follow this traditional route and the main argument for this can be stated as follows:

- In a sparsely fractured rock it is believed that most of the flow is due to a limited number of major fracture zones. The main task is thus to identify these and to represent them in the numerical model. If a refined modelling is required the next size class of fractures or fracture zones should be considered. For a rock block with dimensions 100 x 100 x 100 m^3, all hydraulically active fractures may need to be considered. From this point of view it seems more logical to first consider large fractures, and then progressively smaller ones, than to upscale point measurements.

This is essentially the approach used by discrete fracture network (DFN) models. DFN models also require information from field measurements in order to specify the properties of the fracture network (fracture size distribution and orientation, transmissivities, etc). The flow is then calculated in each fracture individually and there is hence no need to represent the fracture as grid cell conductivities.

One can thus identify two basic approaches in groundwater modelling; in one we define grid cell conductivities (sometimes called the continuum porous-medium (CPM) approach), in the other we calculate the flow through the network directly (DFN approach). Both approaches have their merits and drawbacks, which however will not be discussed in this report. Instead we will try to combine the approaches, meaning that we first generate a fracture network and then represent the network as grid cell conductivities. The resulting conductivity fields are expected to have some desirable properties, like realistic correlation and anisotropy structure, provided the network is properly represented in the grid. In order to demonstrate the correctness and potential of the method, two studies are carried out. The first one, this report, attempts to show that a single fracture, or a fracture network, can be represented in a computational grid with acceptable accuracy. The second report, Svensson (1999), describes

an application to the Äspö Hard Rock Laboratory (HRL). Here field data are extensively used to specify the fracture network and to calibrate the model. It is recommended that both reports are studied in order to get a full account of the method proposed.

The objective of this report is to establish how well a fracture network can be represented as grid cell conductivities. This will be done by a series of testcases for which analytical solutions or results from theories are available. Altogether five test cases will be analysed.

2 BASIC CONCEPTUAL ASSUMPTIONS

2.1 THE SITUATION IN MIND

The proposed method may not be applicable to all fractured rocks. If, for example, the conductivity is due to small but highly conductive fractures it may be a good approach to generate cell conductivities from a log-normal distribution and neglect possible correlation and anisotropy structures. Another possibility is that relatively few large fracture zones dominate the hydraulic properties of the rock. This is the expected situation at Äspö (Rhén et al., 1997). In Figure 2-1 the major fracture zones at Äspö are shown. The properties, location and extension of these zones have been extensively studied and it is believed that they provide the "first order" response in, for example, a pump test. The length scale of the major fracture zones is typically above, say, 300 metres. Fracture zones smaller than 300 metres have also been mapped at Äspö, see for example Figure 2-2, and there is no reason to assume that these can be neglected.

The method is developed with a fracture system of the kind found at Äspö in mind. A recent analysis of LaPointe et al. (1999) shows that the fracture system can be characterised by fractal scaling laws, which indicates that the fracture length distribution can be described by a power law. These features of the fracture system are fully recognised when the fracture network for Äspö is generated, see Svensson (1999).

2.2 GRID CELL CONDUCTIVITIES

Before we discuss how fractures are represented as grid cell conductivities a few characteristics of the computational grid and the fractures need to be introduced. A staggered grid is to be used, which means that scalar quantities, like pressure and salinity, are stored at cell centres while velocity vectors are stored at cell wall centres, see Figure 2-3. Each variable is assumed to be representative for a certain control volume, which is the volume the discretized equations are formulated for. For a velocity cell it is clear that the driving pressure force can be easily formulated. As we are going to apply the Darcy law to the velocity cell we also need a relevant cell conductivity to obtain the cell wall velocity. How to calculate this conductivity is the main subject of this chapter. First, however, we need to define some nomenclature for the fractures, see Figure 2-3. A fracture that has one single opening will in the following be called a single fracture, while a

fracture zone consists of several crossing fractures. For a single fracture we call the width of the opening the aperture, which is typically less than 10^{-3} metres. For a major fracture zone the width is typically 10 metres. In the present study we will make no distinction between a single fracture and a fracture zone; both are idealised as a block with dimensions H (height), W (width) and L (length). In Figure 2-3 also the fracture centre plane is defined; for 2D cases a corresponding fracture centre line can be defined. If the transmissivity of the single fracture, or the fracture zone, is denoted T we can define the hydraulic conductivity of the block as $K = T / W$. In the following we will call the conductive block a fracture. The key idea of the method can now be stated as follows:

- Fractures are assumed to have a width and a conductivity. A fracture contributes to the conductivity of a velocity cell by an amount which is equal to the intersecting volume times the conductivity of the fracture. Contributions from all fractures that intersect the velocity cell are added and the sum is divided by the cell volume. This gives the velocity cell conductivity.

Some illustrations of the concept of intersecting volume can be found in Figure 2-4. For a small fracture the intersecting volume may be the fracture volume, while for a large fracture the cell volume can be the intersecting volume. The basic principle of the method is obviously very simple but, as will be demonstrated in this report, still general enough to handle even complex fracture networks. A few properties of the method can already at this stage be identified:

- All cell wall conductivities will be different, as we generate three conductivity values for each scalar cell. A conductivity field that is anisotropic on the cell scale is hence always generated.

- A fracture smaller than the cell size can not generally contribute to the anisotropy or correlation of the conductivity field.

2.3 A FIRST ESTIMATE OF ACCURACY

Some calculations (which can be done without a computer) for 2D cases will now be presented; these cases illustrate the basic idea and also give a first estimate of the accuracy that can be expected.

Various fractures that intersect a velocity cell are shown in Figure 2-5. It is also shown how the conductivity of the velocity cell is calculated. For the cases shown the cell conductivity is calculated correctly, meaning that a correct flux is obtained through the fracture. However, for thin fractures this may not always be the case. If the fractures are aligned with a coordinate direction, or at an angle of 45° to the

coordinate directions, it can be shown that a correct flux is obtained. For other angles a correct flux is obtained or a small error (resulting in an error of a few % in the calculated flow rate) may occur. In the worst case found the fracture centre line has an equation like $y = 0.5x + 0.25$ (in the coordinate system shown in Figure 2-5). If the fracture is very thin ($W / \Delta << 1$, where Δ is the size of the grid cell) a flux of 83.3% of the correct one is obtained. The accuracy increases however rapidly if the fracture is made thicker. For $W / \Delta = 0.25$ the flux ratio is 0.925 and for $W / \Delta = 0.89$ it is 0.986. We learn from these calculations that the fracture width, W, in relation to the cell size, Δ, is affecting the accuracy of the representation.

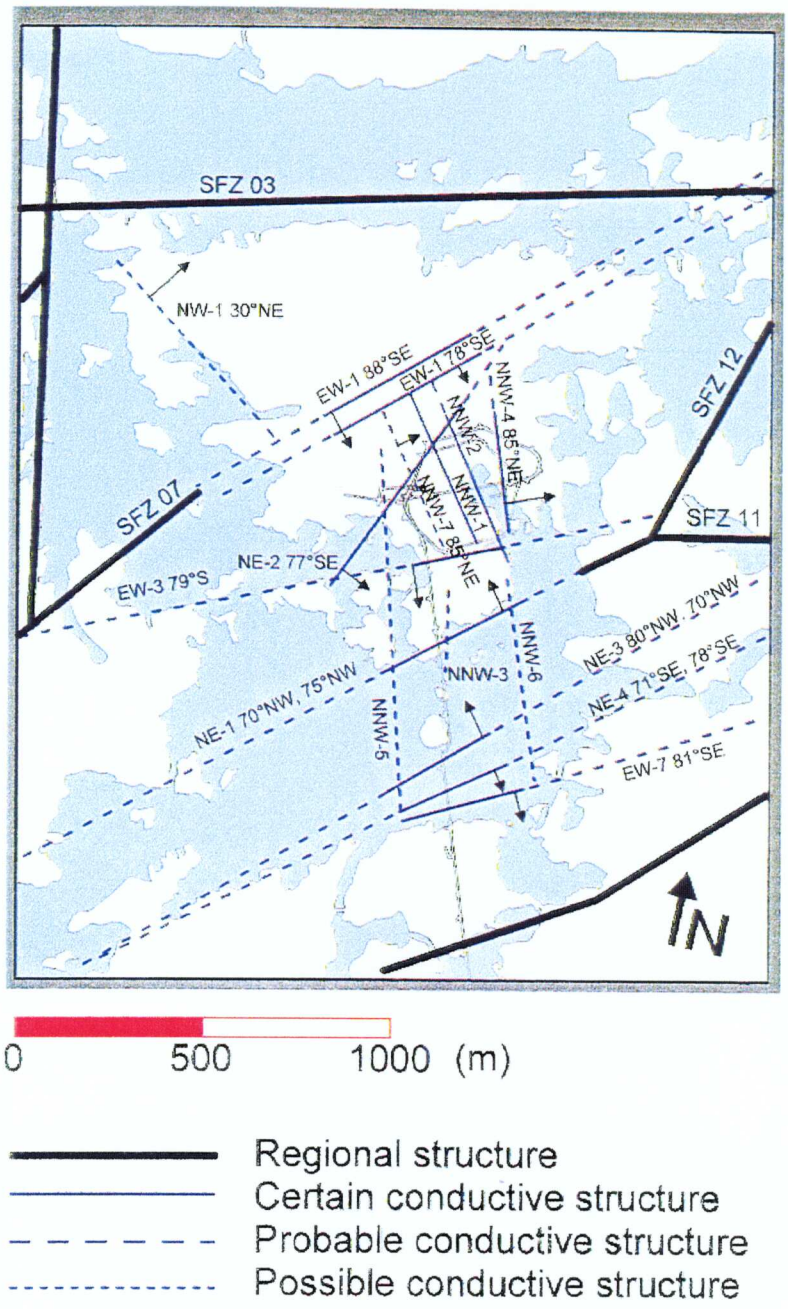

Figure 2-1. *Major fracture zones in the area, after Rhén et al. (1997).*

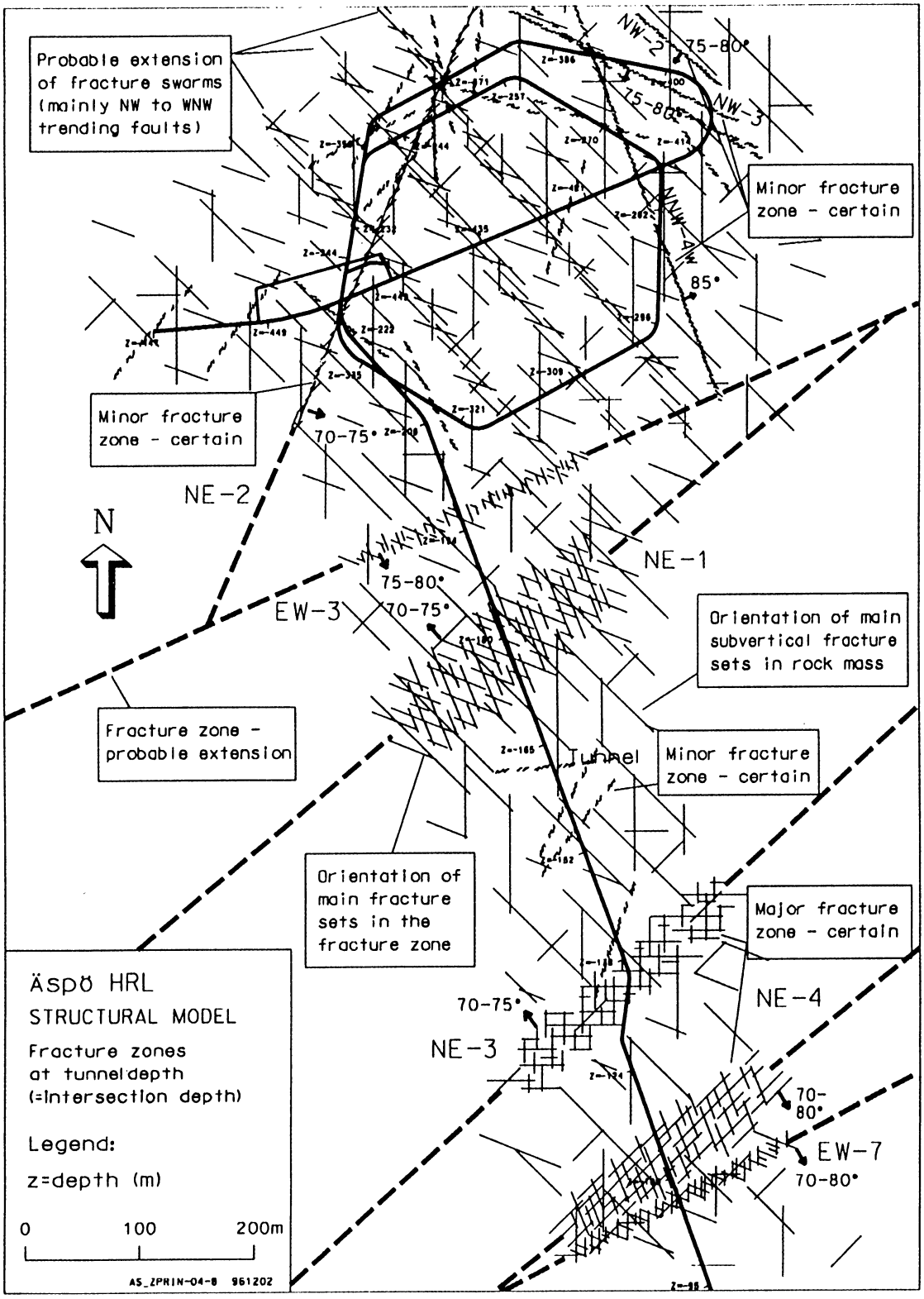

Figure 2-2. *Major and intermediate sized fracture zones on southern Äspö, after Rhén et al. (1997).*

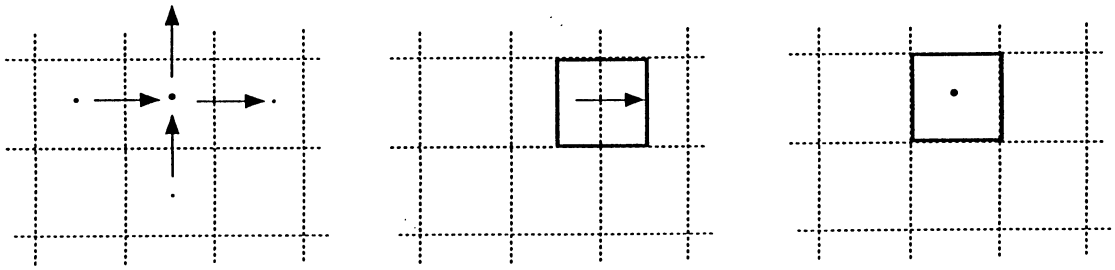

STAGGERED GRID

CONTROL VOLUME FOR VELOCITY

CONTROL VOLUME FOR SCALAR

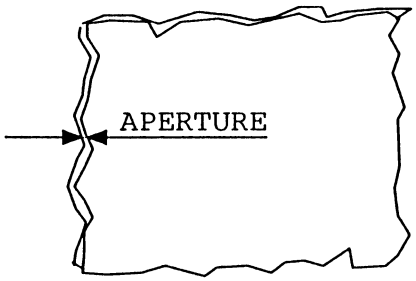

SINGLE FRACTURE

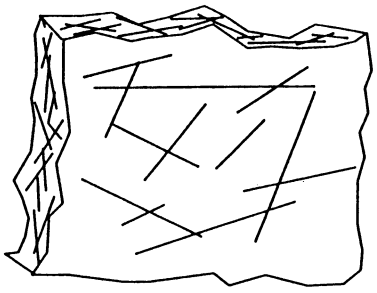

FRACTURE ZONE

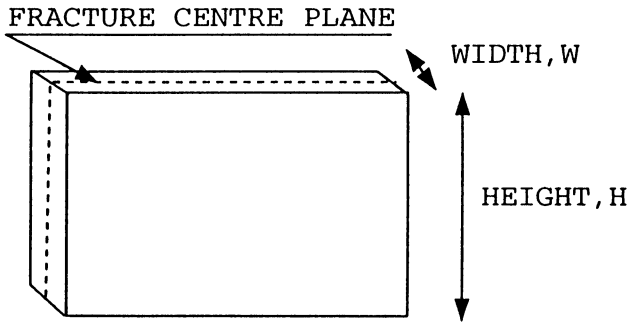

ASSUMED FRACTURE GEOMETRY

Figure 2-3. *Some features of the computational grid (top) and some definitions of the fracture geometry.*

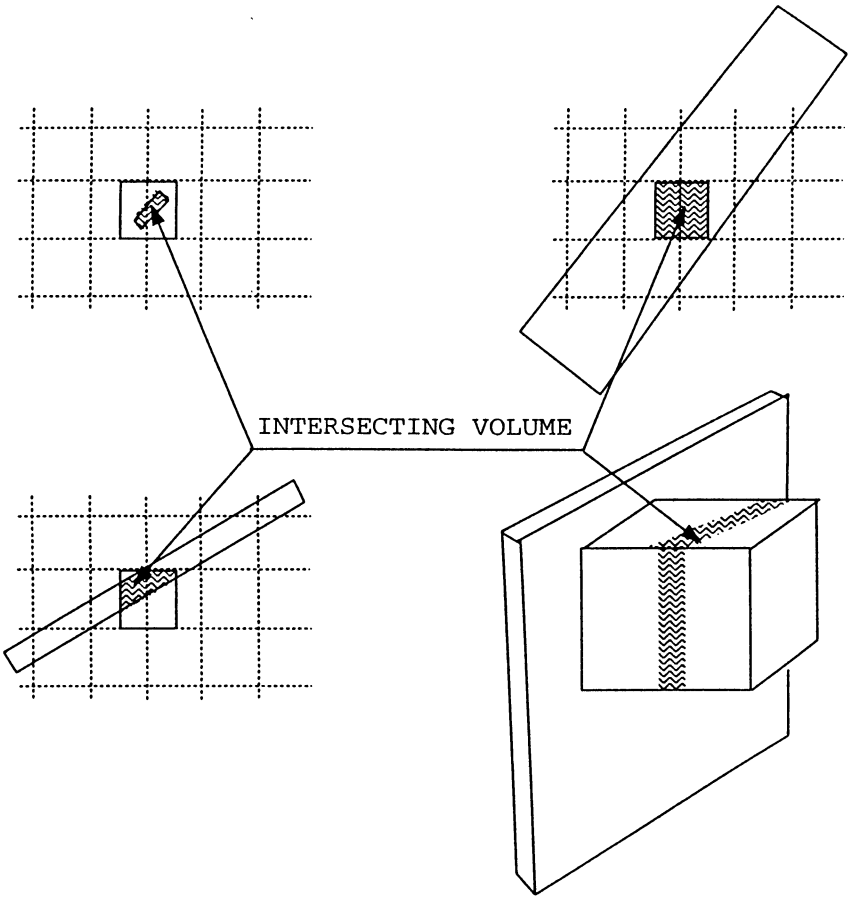

Figure 2-4. *Illustration of the concept of intersecting volume. The shaded area indicates the volume that intersects a velocity cell.*

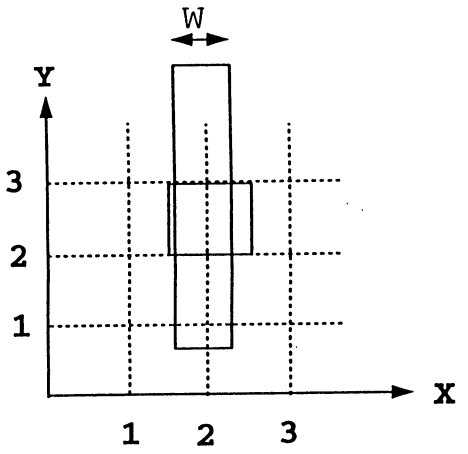

$$COND = W\Delta K / \Delta^2$$

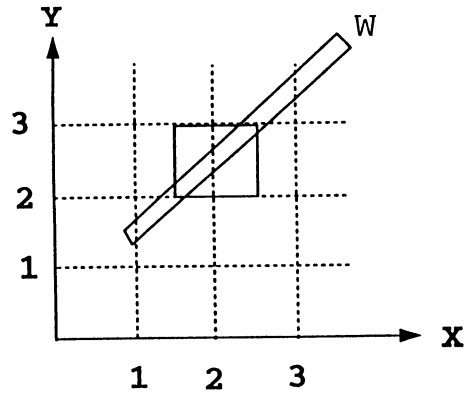

$$COND = W\sqrt{2}\Delta K / \Delta^2$$

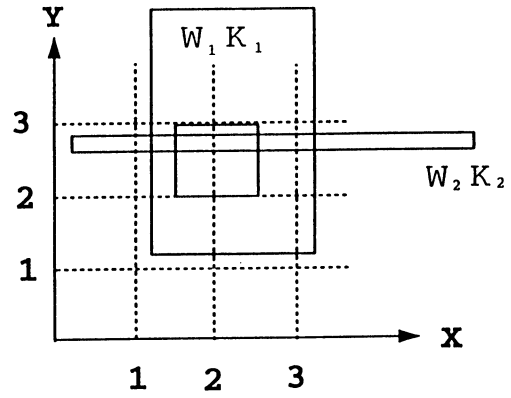

$$COND = \left(K_1\Delta^2 + K_2 W_2 \Delta\right)/\Delta^2$$

Figure 2-5. *Illustration of how fracture zones are represented as grid cell conductivities in some simple 2D cases.* Δ *denotes grid size,* K *conductivity and* W *the fracture zone width.*

3 MATHEMATICAL MODEL

3.1 BASIC ASSUMPTIONS

It will be relevant to assume that the fluid is incompressible and the flow is steady for all testcases to be discussed. We will further assume that the Darcy law applies and that no forces due to density gradients are present.

3.2 GOVERNING EQUATIONS

Under the assumptions made the following equations apply:

Momentum:

$$0 = -\frac{\partial p}{\partial x} - \frac{\rho_0 g}{K_x} u \tag{3-1}$$

$$0 = -\frac{\partial p}{\partial y} - \frac{\rho_0 g}{K_y} v \tag{3-2}$$

$$0 = -\frac{\partial p}{\partial z} - \frac{\rho_0 g}{K_z} w \tag{3-3}$$

Mass balance:

$$\frac{\partial}{\partial x}\rho_0 u + \frac{\partial}{\partial y}\rho_0 v + \frac{\partial}{\partial z}\rho_0 w = 0 \tag{3-4}$$

where u, v and w are Darcy velocities, K_x, K_y and K_z conductivities, p pressure, g acceleration due to gravity and $\rho_0 \left(= 1000\ \mathrm{kg/m^3}\right)$ density. The coordinate directions are denoted x, y and z.

3.3 BOUNDARY CONDITIONS

Two types of boundary condition will be used; prescribed pressure and zero mass flux. In many of the test cases pressure is

prescribed for two opposite faces of the computational domain and a zero flux condition is used for all other boundaries.

3.4 NUMERICAL TOOL AND OUTPUT PARAMETERS

The system of equations is solved by the general equation solver PHOENICS (Spalding, 1981). PHOENICS is based on a finite-volume formulation of the basic equations and embodies a wide range of coordinate systems (cartesian, body-fitted, cylindrical, etc) and numerical techniques (higher order schemes, solvers, etc).
The basic output parameters from the model are pressure and Darcy velocities. It is however simple to generate additional output parameters like hydraulic head.

4 RESULTS

4.1 INTRODUCTION

Five testcases have been designed for the evaluation of the suggested method. The first three cases deal with situations for which analytical solutions are available. Quantitative comparisons can thus be made. The two last testcases compare the simulated results with those from established theories.

In all cases we will use a computational domain, 2D or 3D, with a sidelength of 100 metres. The cell size Δ is 1 metre if not otherwise stated. For computational reasons a small background conductivity is added to all cells. This conductivity was given a value of 10^{-12} m/s; a value small enough to give a negligible contribution to the flow through the domain. Further details will be given separately for each test case.

In Section 2 it was shown that the accuracy of the method is related to W / Δ, i.e. the fracture width in relation to the cell size, and the angles the fracture forms with the coordinate directions. These aspects will therefore be in focus in the first three test cases.

4.2 A SINGLE FRACTURE IN A 2D DOMAIN

The first case to be discussed deals with a fracture that runs along the coordinate directions, see Figure 4-1. We expect that the fracture transmissivity should be correctly represented in this situation. The main task is therefore to evaluate if a correct pressure distribution can be obtained. As can be seen in Figure 4-1, the global pressure gradient is in a diagonal direction. It can also be understood that a local pressure gradient that is in the opposite direction needs to be generated in order to drive the flow through the fracture.

The coordinates for the centreline of the fracture are given in Figure 4-1; the total length along the centreline is 360 metres. The centreline does however not represent the mean streamline in the right angled bends of the fracture, see Figure 4-1. As the fracture width will be represented in two cells in the grid (to be discussed further below) a quarter of a circle (with a radius of 2Δ) is a better representation of the flow around a corner. With this assumption the total length of the

mean streamline is 355.3 metres; this is the value to be used when the simulated transmissivity is evaluated.

The calculated pressure distribution is shown in Figure 4-2. As can be seen a complex pattern is obtained, but the pressure drop along the centreline of the fracture is linear, as expected.

The most direct way to analyse the simulations would be to compare the calculated flow through the fracture, Q, with the corresponding flow given by the analytical solution. However, we can not obtain the exact analytical solution due to the uncertainty about the mean streamline length, discussed above. Instead we choose to compare the simulated mean transmissivity of the fracture, T, with the prescribed transmissivity, T_0, which is equal to the prescribed conductivity times the fracture width. The simulated mean transmissivity can be evaluated from:

$$T = Q / \frac{dh}{L} \tag{4-1}$$

where Q is the calculated flow through the fracture, dh the prescribed head difference (= 1 metre) between the inlet and outlet sections and L (= 355.3 metres) the total length of the average streamline, discussed above. The ratio T / T_0 is given for different fracture widths in Table 4-1. As can be seen a very close agreement is found.

In Table 4-1 it is seen that T / T_0 is 1.005 for $W / \Delta = 2.0$ but 0.999 for all other widths. This result can be explained by considering how the fracture is represented as grid cell conductivities. In Figure 4-3 the two situations are illustrated. When $W = 2\Delta$ conductivities for velocity cells are generated that allow a shortcut around the corner. For $W \leq \Delta$ this shortcut is closed; in fact all fractures with $W \leq \Delta$ will be represented in the same cells, which explains why T / T_0 is constant for these widths.

Table 4-1. Fracture transmissivity as represented in the grid, T, normalised with the true, prescribed transmissivity, T_0, versus fracture width, W.

W/Δ	T/T_0
2.0	1.005
1.0	0.999
0.5	0.999
0.25	0.999
0.125	0.999

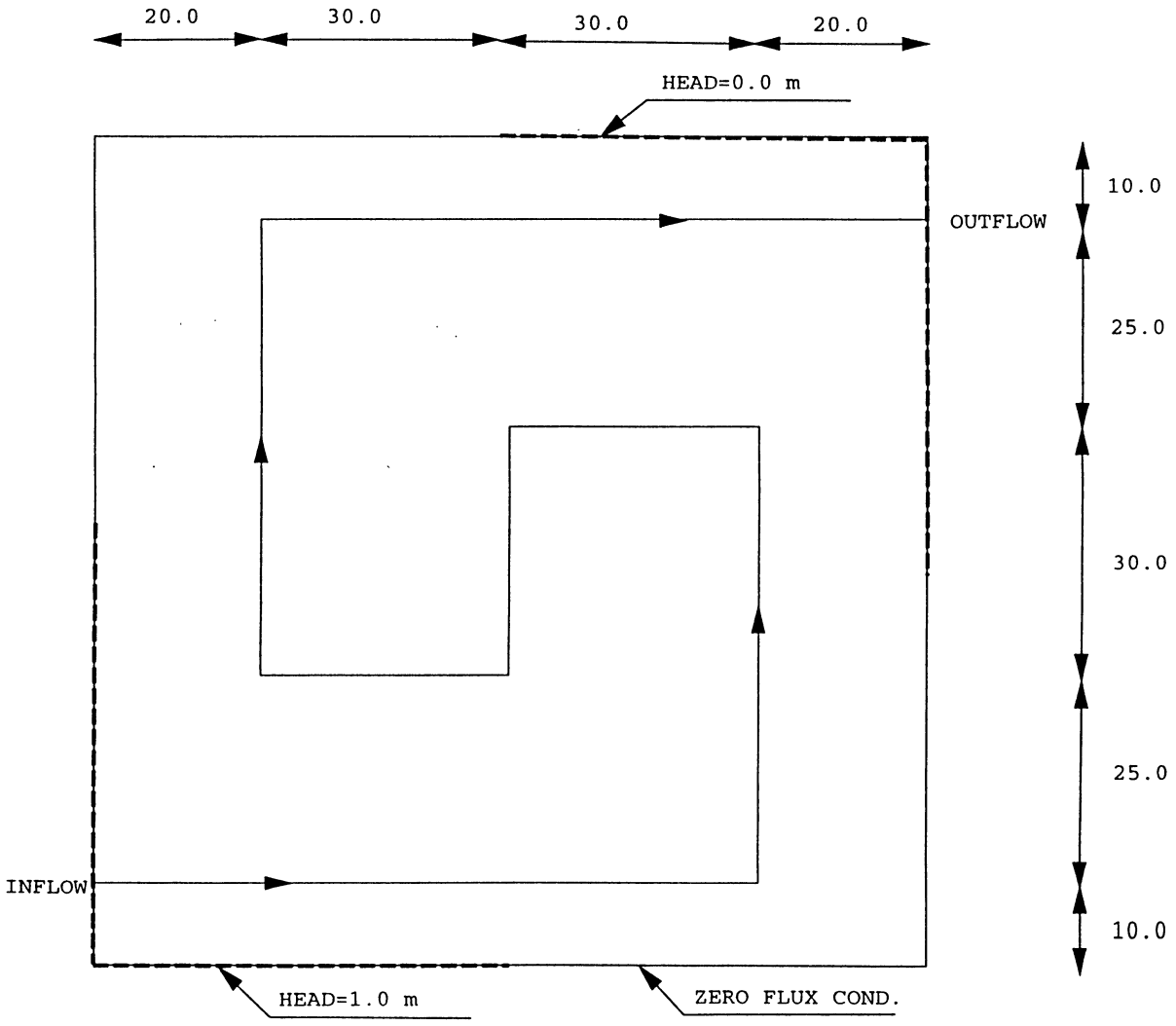

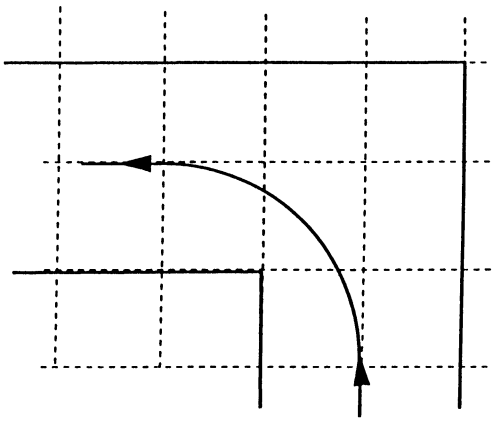

MEAN STREAMLINE IN A BEND

Figure 4-1. *A single fracture in a 2D domain. Outline of situation studied and coordinates for centreline of the fracture (top) and assumed mean streamline path in right-angled bends. All distances in metres.*

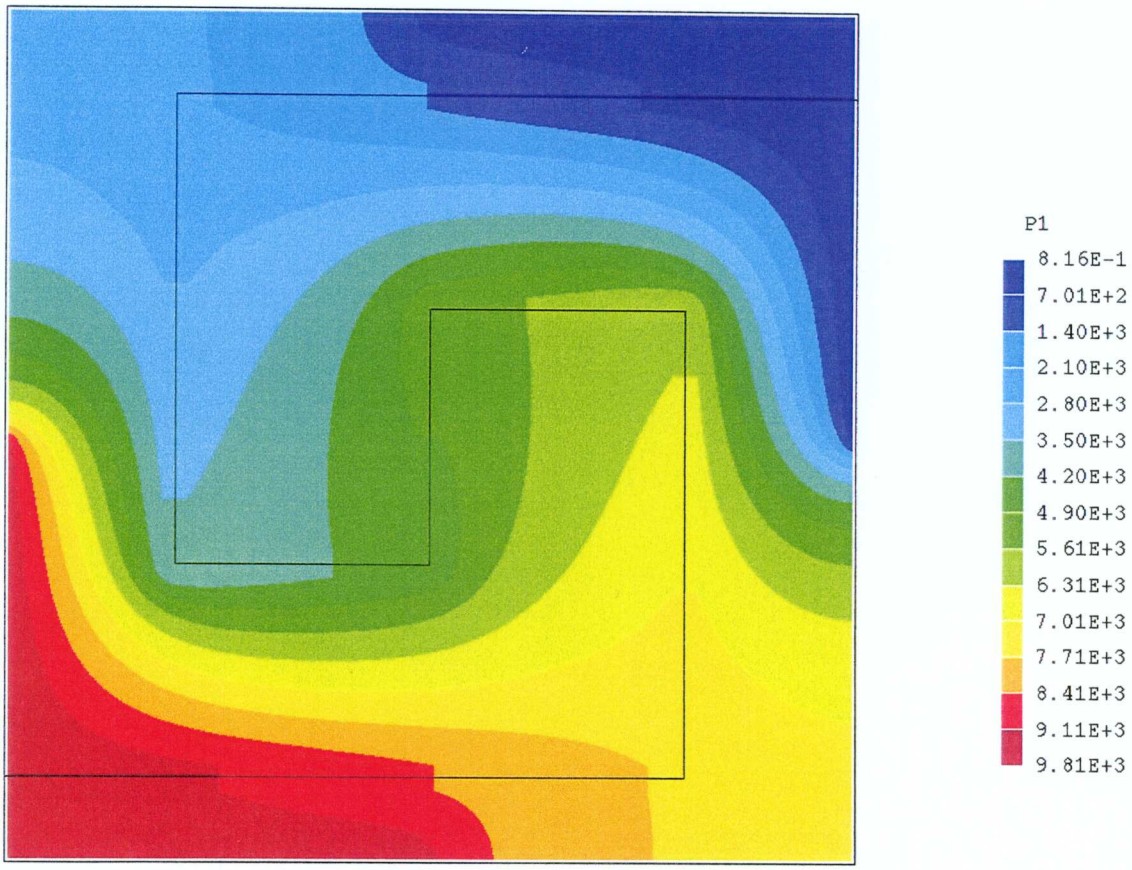

Figure 4-2. *A single fracture in a 2D domain. Pressure distribution. Solid line indicates centre line of fracture.*

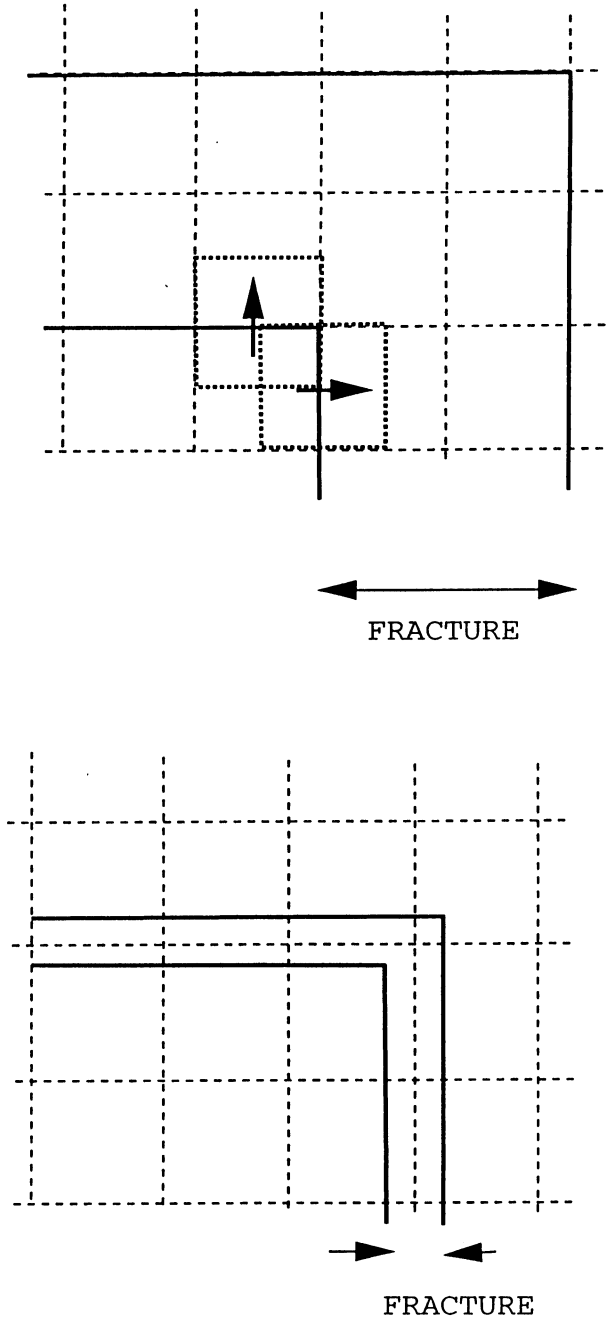

Figure 4-3. *A single fracture in a 2D domain. If* $W = 2\Delta$ *(top figure) a shortcut is generated for the corner velocity cells.*

4.3 A SINGLE FRACTURE IN A 3D DOMAIN

It was noted in Section 2.3 that the accuracy of the representation of a fracture is depending on the angles the fracture forms with the coordinate directions and the width of the fracture (in relation to the cell size Δ). The purpose of this testcase is to establish the magnitude of the errors that can be expected due to these effects.

The situation studied is outlined in Figure 4-4. The pressure is held constant on two opposite faces ($y = 0.0$ m and $y = 100.0$ m) and a zero flux condition is used on all other boundaries. At the inflow boundary the position of the fracture is fixed, with centreline coordinates (10.0, 0.0, 10.0). The fracture position at the downstream boundary is varied in order to test a wide range of angles to the coordinate directions. Also a range of widths were tested, but the height of the fracture was kept constant at 5 metres.

Results are presented in Table 4-2. Five downstream fracture positions and five fracture widths were tested. The five downstream fracture positions will give a fracture that, for the first position, is parallel to the y- coordinate while the last position gives a fracture that almost follows a diagonal in the box. Note also that the x and z coordinates for the downstream positions are different; this ensures that the fracture will have different angles to all three coordinate directions (except for the first position). The grid representation of the transmissivity, T, is obtained from the calculated flow rate, the pressure difference between the inlet and outlet planes and the centreline length of the fracture. In Table 4-2 the ratio T/T_0, where T_0 is the true, prescribed, transmissivity, is given for the five downstream positions and fracture widths. For the first position, i.e. the fracture that is parallel to the y-coordinate, the transmissivity is represented exactly in the grid. For other angles it is found, as expected, that the error generally increases with decreasing W / Δ. In Table 4-2 also the average T/T_0 as a function of W / Δ can be found. The average ratio for all 25 tested situations is 0.986.

A comment may be needed to the value 1.005 ($x = 90$, $z = 70$, $W / \Delta = 2.0$) in Table 4-2. It is expected that the method gives $T / T_0 \leq 1.0$ for all widths and all angles the fracture forms with the coordinates. The explanation for values larger than 1.0 is that the mean streamline may be shorter than the centreline of the fracture, see Figure 4-4. The T-values in Table 4-2 were all calculated using the centreline of the fracture as the distance between the inlet and outlet plane and may hence overestimate the length somewhat.

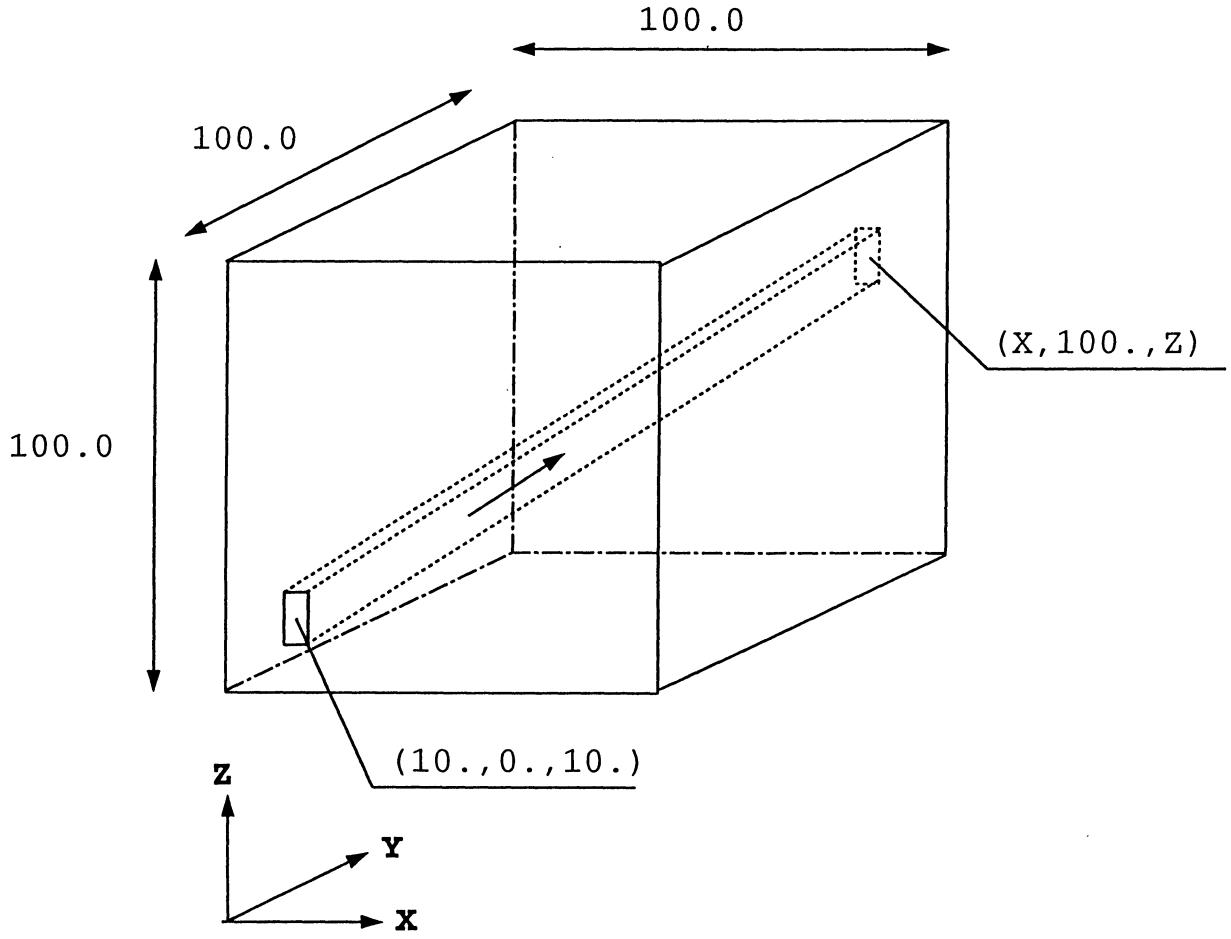

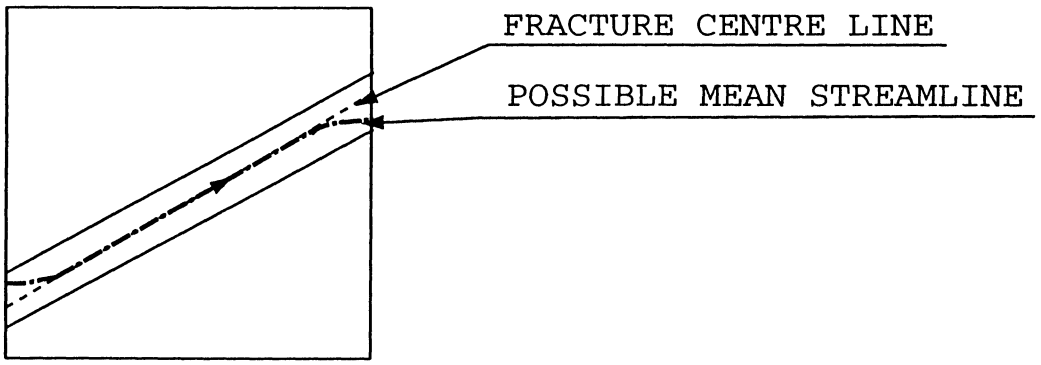

Figure 4-4. *Single fracture in a 3D domain. Outline of situation studied (top) and illustration of fracture centre line and mean streamline. All distances in metres.*

Table 4-2. Single fracture in a 3D domain. The transmissivity as represented in the computational grid, T, normalised with the true transmissivity, T_0, for various fracture widths and orientations.

Fracture coordinates at downstream boundary [m]	Transmissivity ratio, T/T_0				
	Fracture width, W/Δ				
	2.0	1.0	0.5	0.25	0.125
x = 10.0, z = 10.0	1.000	1.000	1.000	1.000	1.000
x = 30.0, z = 25.0	0.996	0.992	0.980	0.953	0.950
x = 50.0, z = 40.0	0.996	0.989	0.970	0.948	0.966
x = 70.0, z = 55.0	1.000	0.994	0.984	0.971	0.968
x = 90.0, z = 70.0	1.005	0.999	0.996	0.993	0.989
Average	0.999	0.995	0.986	0.973	0.975

4.4 MANY FRACTURES IN A 3D DOMAIN

The next case to be discussed deals with many fractures that may cross each other. The computational domain is the same as in the previous case, see Figure 4-4. In the present case we will however include many fractures with start and end positions randomly distributed on the inlet and outlet boundaries. The purpose of the testcase is thus to evaluate how well we can predict the transmissivity of several, randomly oriented, crossing fractures.

As in the previous cases a range of widths will be considered, but the height of the fractures will be held constant and equal to 5 metres. 25 fractures will be generated with start and end positions randomly distributed on the squares $10.0 < x < 90.0$, $10.0 < z < 90.0$. The total flow rate, Q_t, will be equal to the sum of the flow in each fracture:

$$Q_t = \sum Q = \sum HT \frac{\Delta h}{L} = HT\Delta h \sum \frac{1}{L} \qquad (4\text{-}2)$$

In order to calculate the average fracture transmissivity as represented in the grid, T, we need to know the total flow rate and the sum of the inverted fracture lengths. These lengths are calculated and stored during the generation of the fractures. The generated fracture system, consisting of 25 fractures, is shown in Figure 4-5. As can be seen a complex system of crossing fractures is generated. Simulations were carried out for a range of fracture widths and the average fracture transmissivity, T, was estimated from equation (4-2). The result is found in Table 4-3. As for the other testcases, we find that the error increases with decreasing fracture width. For $W/\Delta = 2.0$ the ratio $T/T_0 > 1$; this is probably due to the estimate of the mean streamline length, discussed in the previous testcase.

The last comparison with an analytical solution concerns a situation with varying fracture-sections. In the case discussed above all fractures had the same cross-section. Now we let the height of the fracture vary randomly from 1.0 to 10.0 metres and further assume that the width is 10% of the height. For this case we evaluate the simulated fracture conductivity, K, using the following relation:

$$Q_t = \sum Q = \sum KHW \frac{\Delta h}{L} = K\Delta h \sum \frac{HW}{L} \qquad (4\text{-}3)$$

When we generate the fracture system we calculate and store $\sum HW / L$. With Q_t obtained from the simulation we can estimate the average fracture conductivity, as represented in the grid. Using 25 fractures, illustrated in Figure 4-6, we obtain $K / K_0 = 0.999$, where K_0 is the true fracture conductivity.

Table 4-3. Many fractures in a 3D domain. The average transmissivity as represented in the computational grid, T, normalised with the true transmissivity, T_0, for a range of fracture widths.

Fracture width W/Δ	Average transmissivity T/T_0
2.0	1.006
1.0	1.000
0.5	0.987
0.25	0.967
0.125	0.955

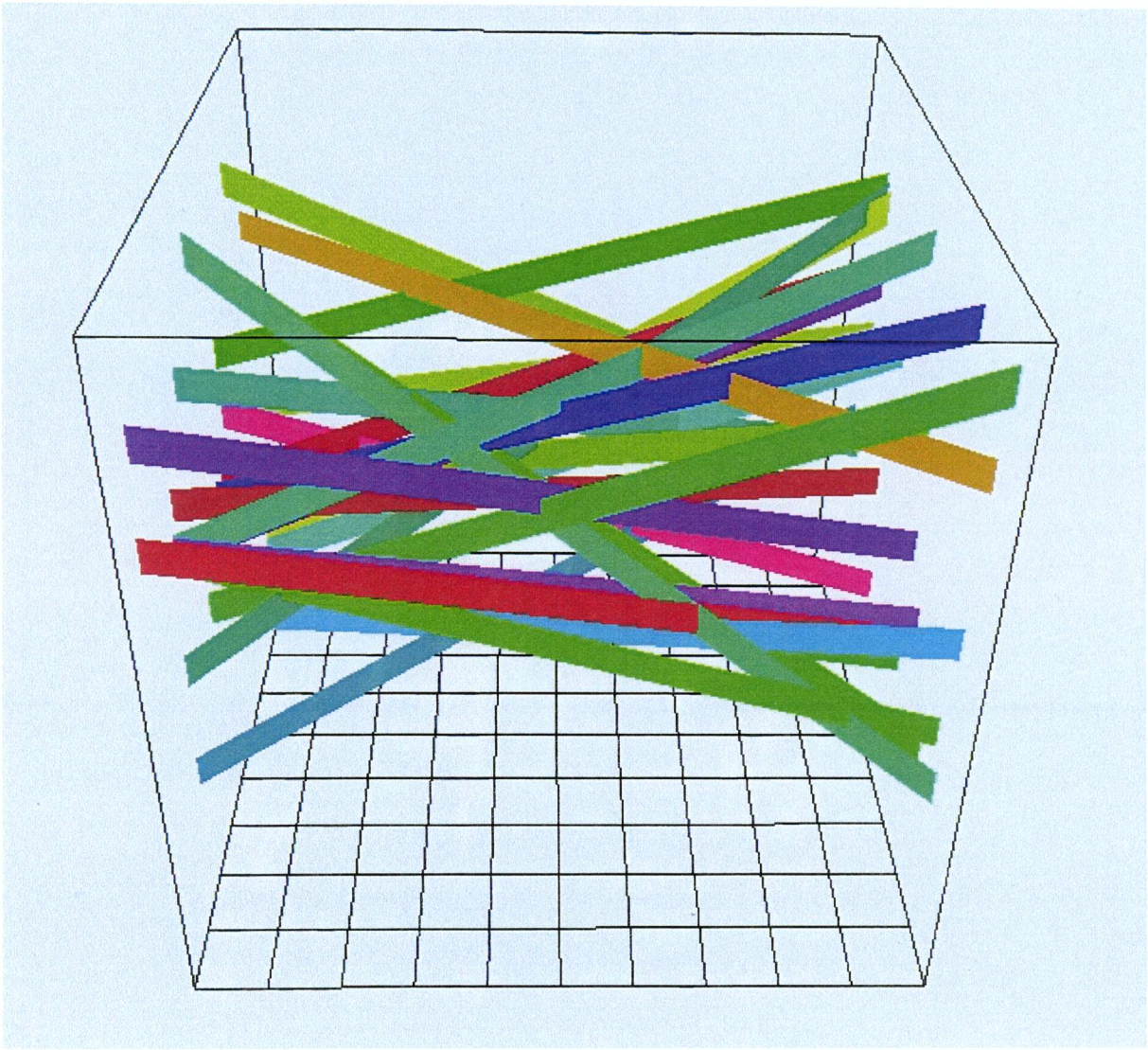

Figure 4-5. *Many fractures in a 3D domain. Illustration of the fracture system. The bottom of the box has been marked with a grid. Colours do not indicate any varying property.*

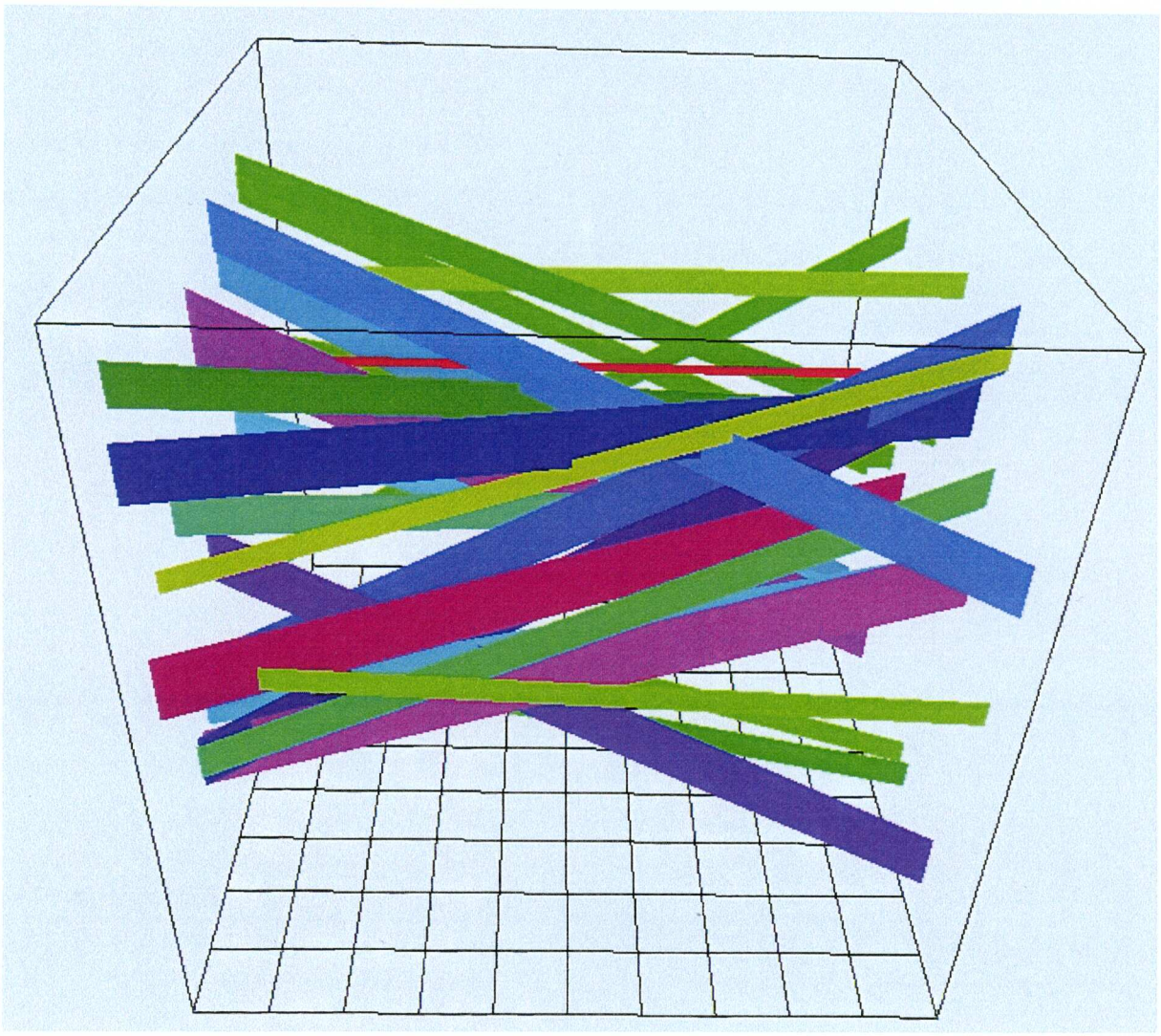

Figure 4-6. *Many fractures in a 3D domain. Colour indicates fracture size with biggest fractures blue and smallest green. The bottom of the box has been marked with a grid.*

4.5 PERCOLATION THEORY

So far we have only considered fractures that directly connect one face of the box with the opposite one. However, in this testcase thin $(W = 0.01\,\mathrm{m})$ square fractures with side lengths of five or ten metres will be distributed randomly in a 100 x 100 x 100 m^3 box. The two main objectives of the testcase are:

- The software package includes an algorithm that detects and removes isolated fractures, or fracture clusters. The algorithm is not exact but may in some cases regard two fractures that are close, but separated, as being in contact. It needs to be verified, by visual inspection of a fracture network, that the algorithm does its task with acceptable accuracy.

- Below a certain fracture density, d, (number of fractures per unit volume) the box faces are not connected, while they are connected through the fracture network above this value. The critical density, d_c, is called the percolation threshold. Estimates of d_c for various fracture networks can be found in the percolation literature and we want to ensure that our fracture network connects the box faces at the correct fracture density.

In a numerical simulation only finite size systems can be considered, while theoretical estimates of d_c often assume infinite systems. Many studies are also restricted to orthogonal fracture sets; a recent example is Bour and Davy (1998). Fewer results are available for the situation we have in mind. However, in Robinson (1984) randomly oriented square planes in a finite volume are studied and a critical density is given. The percolation criterion was that all six faces should be connected by one single cluster. The critical density given by Robinson for a box of 20 x 20 x 20 m^3 filled with thin squares of side length one metre is 1.231 planes per unit volume; this value will be used as a reference.

A fracture network, at the critical fracture density, is shown in Figure 4-7. The fracture length is 5 metres; the fractures have random positions and orientations. The corresponding network for fracture length 10 metres is found in Figure 4-8. In both figures all isolated fractures and fracture clusters have been removed. By careful visual inspection (different view angles, close up views, etc) it is possible to conclude that no isolated fractures are left. It is harder to conclude that no isolated fracture clusters are kept; visually it was however not possible to find any.

Next we consider the question of critical fracture density, d_c. As both the fracture positions and orientations are randomly distributed one realises that d_c can only be given as a probability. For the fracture lengths 5 and 10 metres ten realisations were carried out at three

different fracture densities. The result is summarised in Table 4-4. It will probably take more than ten realisations to get a correct estimate of d_c. However, if we base an estimate of d_c on the fracture density that gives a connection with a probability of 50% we find that $d_c \approx 8\times10^{-3}$ for fracture length 5 metres and $d_c \approx 1.1\times10^{-3}$ for fracture length 10 metres. The corresponding values from the analysis of Robinson (1984) are 9.85×10^{-3} and 1.231×10^{-3}. We can thus conclude that a fair agreement is achieved. In this context it is also of interest to compare our results with the formula given by Charlaix et al. (1984):

$$p = d * \text{ (average area of the fractures)} * \text{ (average half perimeter)} \quad (4\text{-}4)$$

Charlaix et al. (1984) proposed that the dimensionless number p must lie between 1.5 and 3 at the percolation threshold. The present simulations give $p \approx 2.1$, for both fracture sizes, and are hence in good agreement also with this criterion.

Finally some flow simulations will be presented. The purpose of these is to demonstrate that a connected fracture network also results in connected flow channels when the fractures are represented as grid cell conductivities. In order to get clearer illustrations we now use networks that only connect two opposite faces. A head difference is applied over the two opposite faces, while a zero flux condition is used on all other boundaries. A steady state flow calculation is then performed. By plotting an isosurface for the velocity magnitude the flow channels are depicted, see Figures 4-9 and 4-10. As can be seen, the larger fractures can be identified in the flow channels.

Table 4-4. Critical fracture density. For each fracture size and fracture density 10 realisations were tested for connectivity between all six faces of the box.

Fracture size [m]	Fracture density [number per unit volume]	% Connected
5	7.5×10^{-3}	0
	8.0×10^{-3}	70
	8.5×10^{-3}	100
10	1.00×10^{-3}	20
	1.05×10^{-3}	30
	1.10×10^{-3}	90

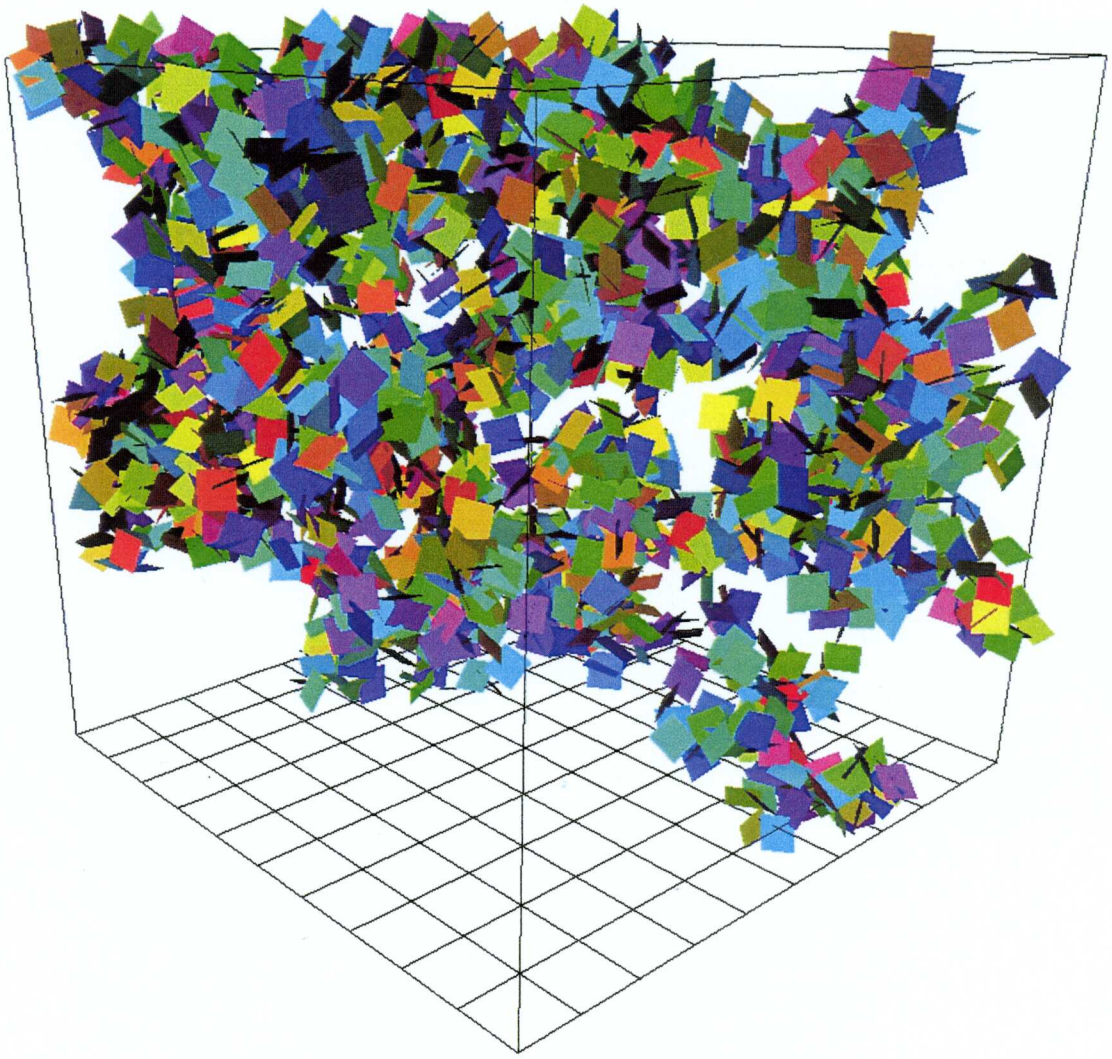

Figure 4-7. *A fracture network that connects all six faces of the box. Fracture density at the percolation threshold. All isolated fractures and fracture clusters have been removed. Fracture size is 5 metres. The bottom of the box has been marked with a grid.*

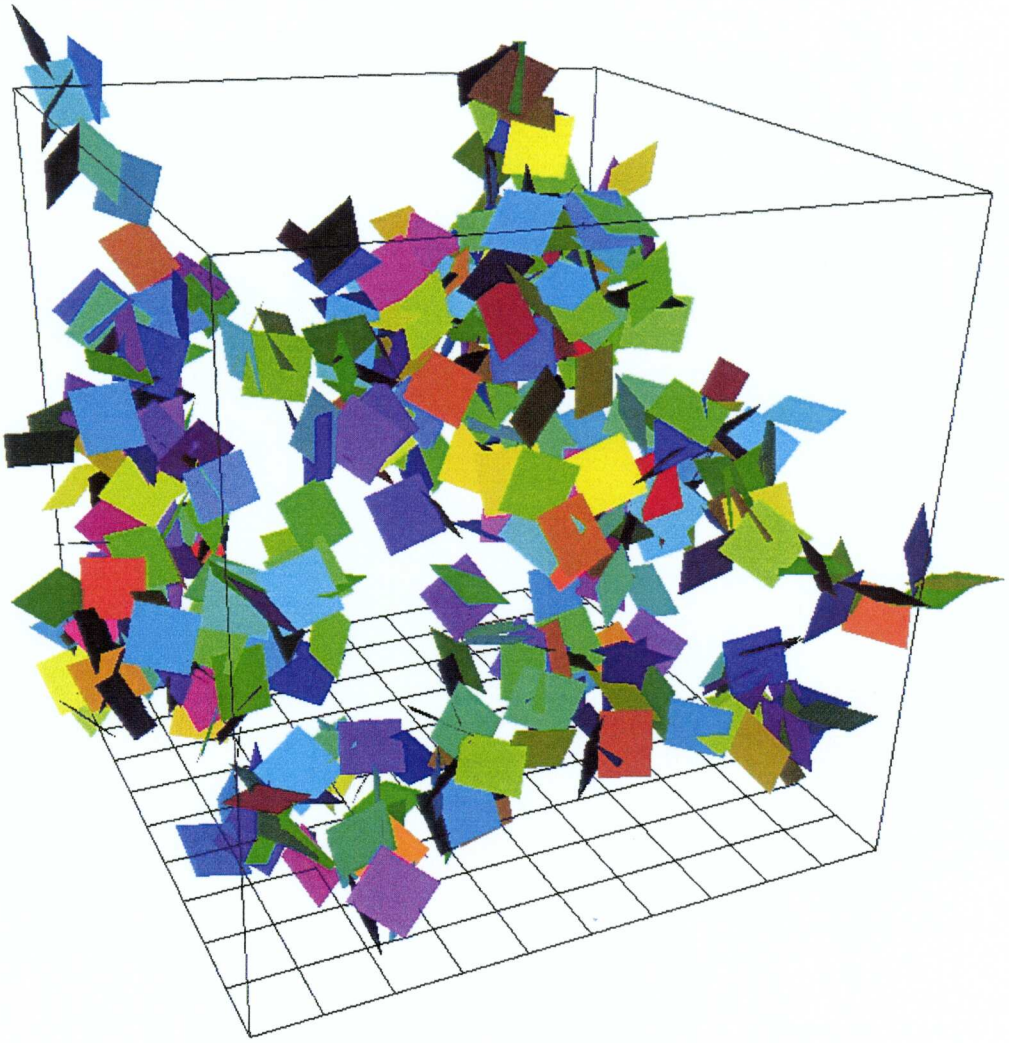

Figure 4-8. *A fracture network that connects all six faces of the box. Fracture density at the percolation threshold. All isolated fractures and fracture clusters have been removed. Fracture size is 10 metres. The bottom of the box has been marked with a grid.*

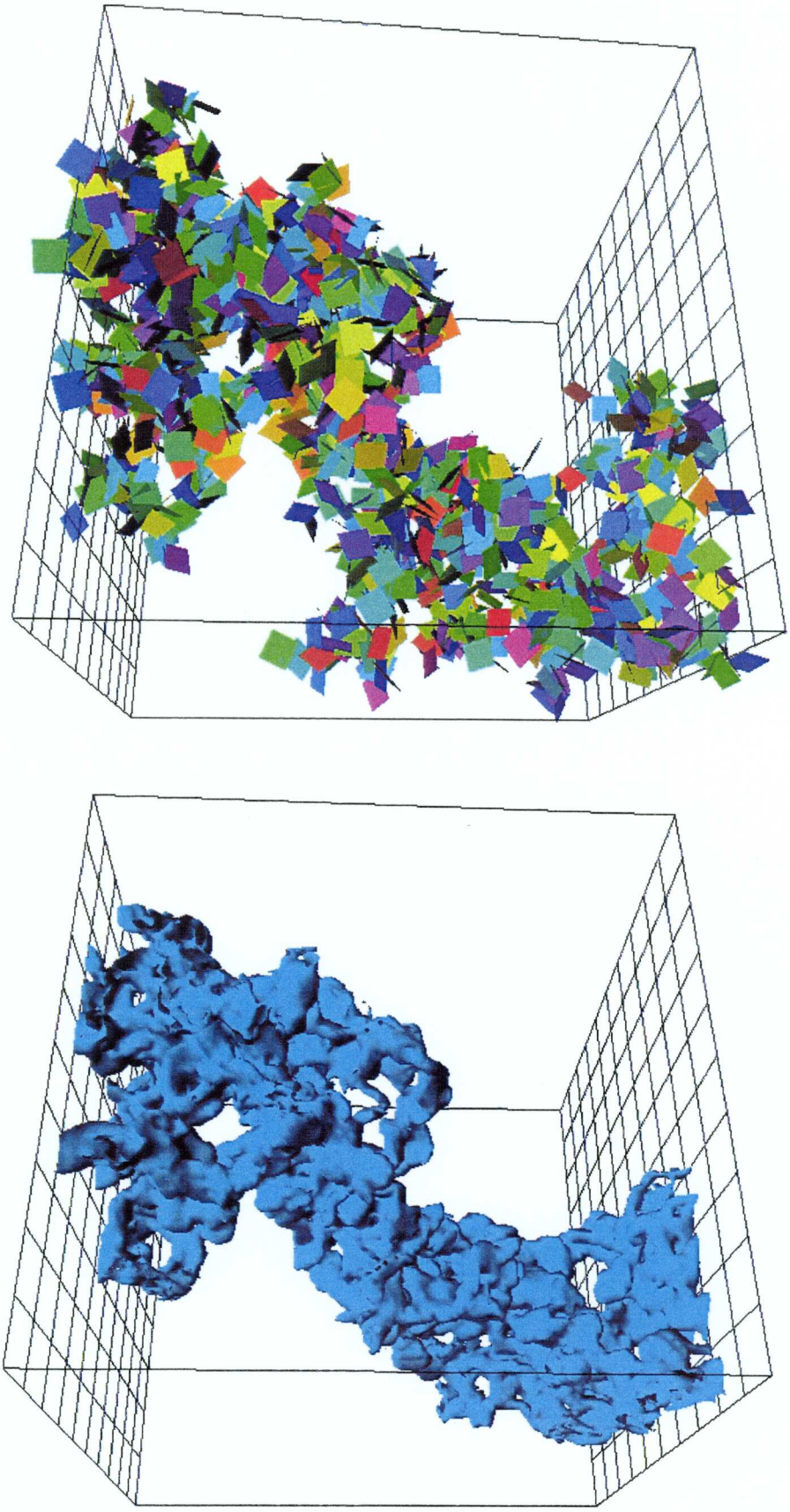

Figure 4-9. *A fracture network that connects two opposite faces of the box (top) and the corresponding flow channels. Fracture density at the percolation threshold. Fracture size is 5 metres. The two connected sides of the box have been marked with grids.*

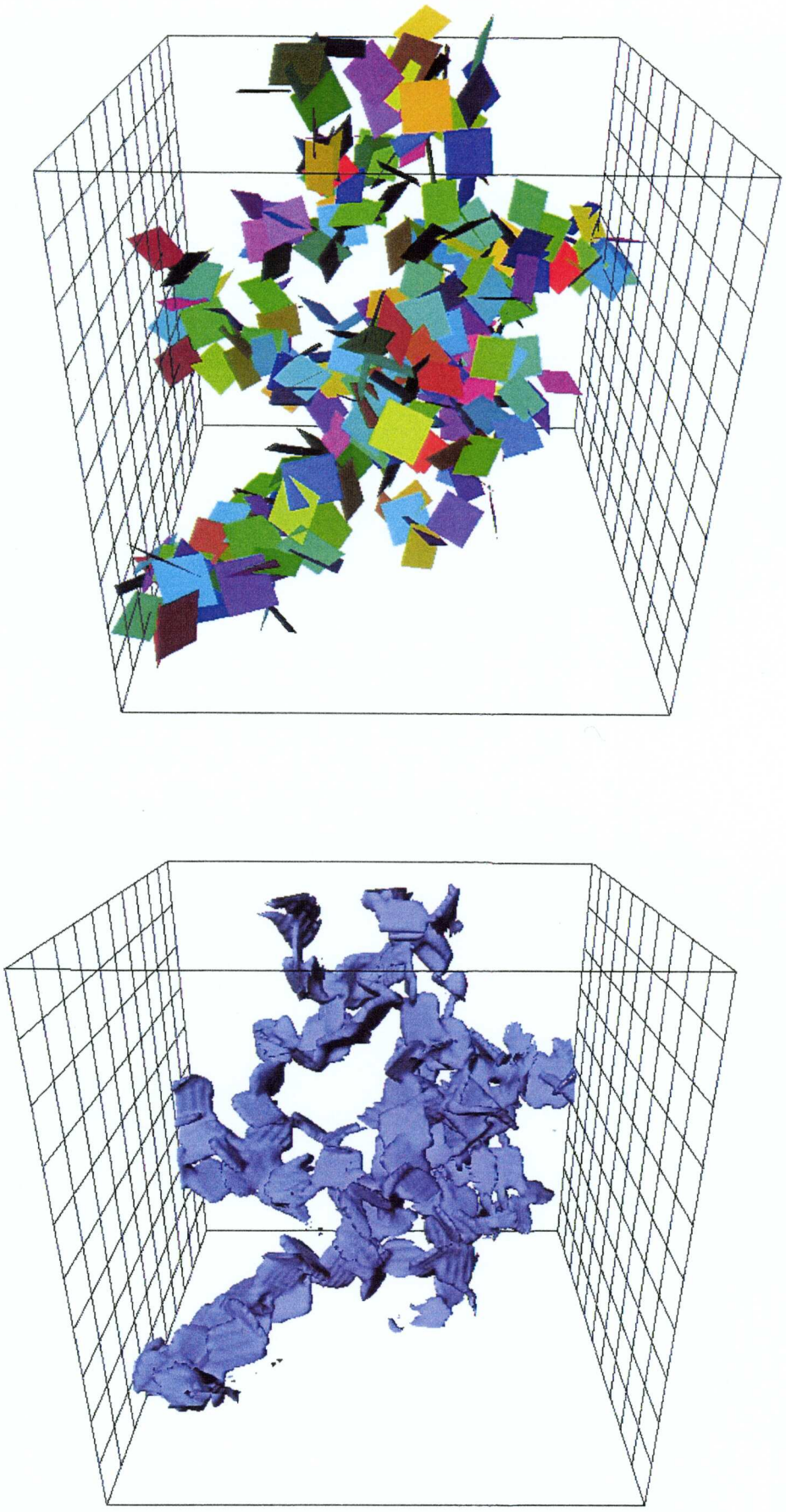

Figure 4-10. *A fracture network that connects two opposite faces of the box (top) and the corresponding flow channels. Fracture density at the percolation threshold. Fracture size is 10 metres. The two connected sides of the box have been marked with grids.*

4.6 EFFECTIVE DOMAIN CONDUCTIVITY

In this testcase we will consider situations with fracture densities well above the percolation threshold, which means that two opposite faces in our computational domain will always be connected. How well the two sides are connected can quantitatively be expressed with the effective domain conductivity, K_{eff}, in the studied coordinate direction. The purpose of this testcase is to verify that K_{eff} is in agreement with available theories on how K_{eff} is related to the properties of the grid cell conductivities.

A thorough review of theories can be found in Renard and Marsily (1997). We will compare simulations with three expressions from this review, assumed to be valid for a stationary, uncorrelated isotropic medium with log-normally distributed cell conductivities.

Matheron (1967):

$$K_{eff} = K_G \exp\left[\sigma^2_{\ln(k)}\left(\frac{1}{2}-\frac{1}{3}\right)\right] \tag{4-5}$$

Gutjahr et al (1978):

$$K_{eff} = K_G\left[1+\sigma^2_{\ln(k)}\left(\frac{1}{2}-\frac{1}{3}\right)\right] \tag{4-6}$$

Dagan (1993):

$$K_{eff} = K_G\left[1+\sigma^2_{\ln(k)}\left(\frac{1}{2}-\frac{1}{3}\right)+\sigma^4_{\ln(k)}\frac{1}{2}\left(\frac{1}{2}-\frac{1}{3}\right)^2\right] \tag{4-7}$$

where K_G is the geometric mean of the grid cell conductivities and $\sigma^2_{\ln(k)}$ represents the variance of the conductivity logarithm.

It is not straight-forward to set up a numerical simulation, whose results can be compared with the theories. This is due to the assumptions mentioned above. As we start with a fracture network a certain correlation will result and it is also hard to ensure that the cell conductivities are log-normally distributed. The following assumptions and specifications of the simulations should be noted:

- The fractures are randomly distributed and oriented, which gives an isotropic conductivity field globally; on the cell scale an anisotropic field will however be generated.

- Two fracture sizes (5 and 10 metres) will be tested. The fractures are square and thin ($W = 0.01$ metre). This gives an indication of how sensitive the results are to the correlation length.

- By prescribing a log-normally distributed fracture transmissivity a fair agreement with the condition concerning log-normally distributed cell conductivities can be obtained (to be shown below). This was found simply by trial and error and there is no theoretical justification to this.

- About 10 000 fractures of fracture size 10 metres, and 40 000 of size 5 metres, in a volume of 100 x 100 x 100 m^3 were generated. The reason for using such a high fracture density is that all cell conductivities should be affected by a fracture. If not, the calculation of K_G may be dominated by the small background cell conductivity, used to avoid zero conductivities in the simulations.

- In order to compare the simulations with the theoretical results we need to vary $\sigma_{\ln(k)}$ (calculated from cell conductivities in the simulations). This was achieved by different grid resolutions. Increasing the cell size will reduce $\sigma_{\ln(k)}$.

Now to the results of simulations. First we need to demonstrate that the cell conductivities are log-normally distributed. The fracture transmissivity was put to $10^{-9.0+1.5C}$, where C is a random number from a normal distribution with zero mean and standard deviation 1.0. As mentioned above, this expression was found by trial and error. The resulting distributions of cell conductivities for the two fracture sizes are shown in Figure 4-11. As a straight line indicates a log-normal distribution we can conclude that the cell conductivities are in fair agreement with this distribution. The comparison with the theoretical results is given in Figure 4-12. It is found that the theories show a significant spread for large variances. The curve by Gutjahr et al. (1978) is however only valid for small variances and the departure for large variances is thus expected. The solid line represents present simulations for both fracture sizes. It is found to be below the curves of Dagan (1993) and Matheron (1967). It is interesting to note that De Wit (1995) found that conductivity fields with a correlation structure give a lower K_{eff} / K_G, for a given variance, than the uncorrelated field.

Due to the many uncertainties involved, it is difficult to draw any firm conclusions from this testcase. The following statement may however be valid: "The fracture networks specified, generate cell conductivities that give a relation between K_{eff} / K_G and $\sigma_{\ln(k)}$, that is in qualitative agreement with classical theories".

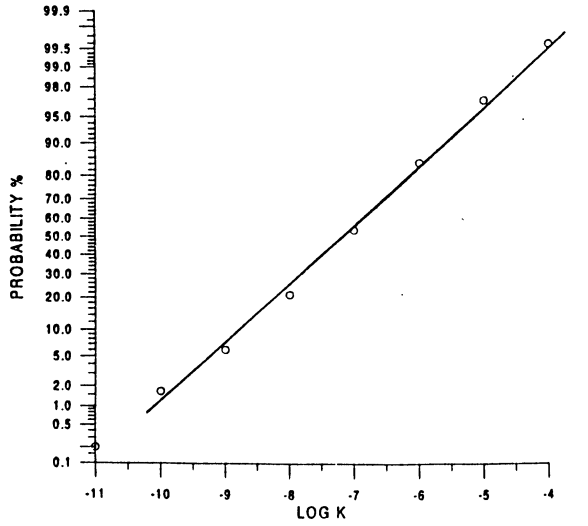

Δ = 2m

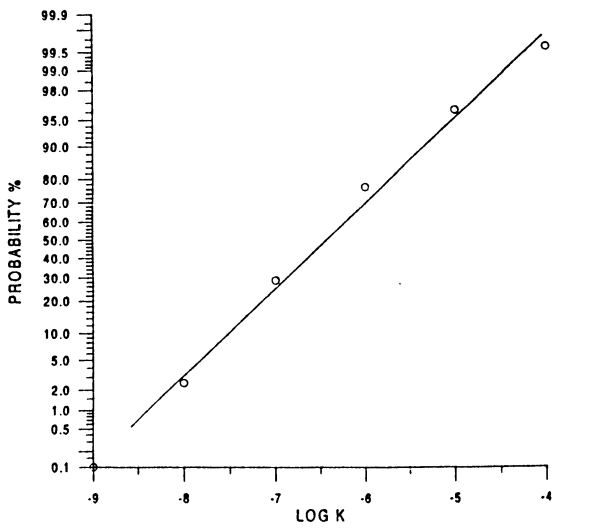

Δ = 4m

L = 5m

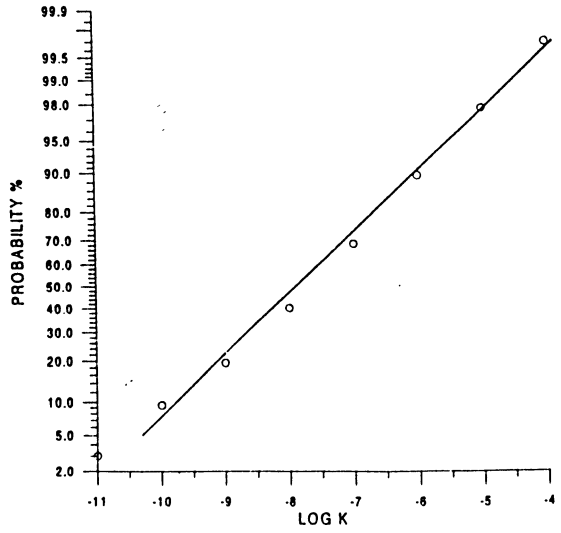

Δ = 2m

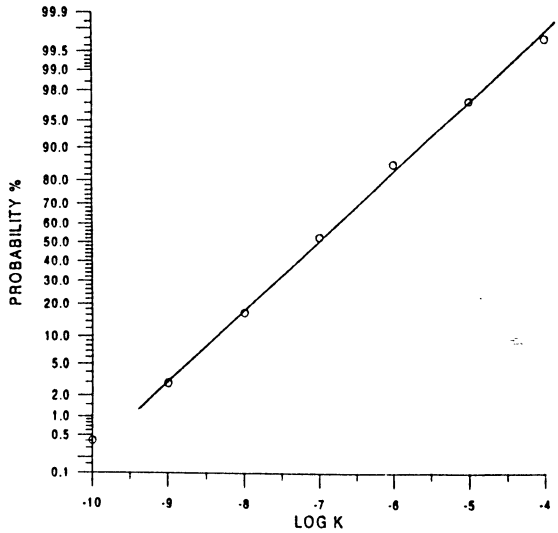

Δ = 4m

L = 10m

Figure 4-11. *Distribution of cell conductivities for a fracture network of 5 metres fractures (top) and 10 metres fractures. Two grid sizes are shown for each fracture size. The straight line in the diagrams indicates a log-normal distribution.*

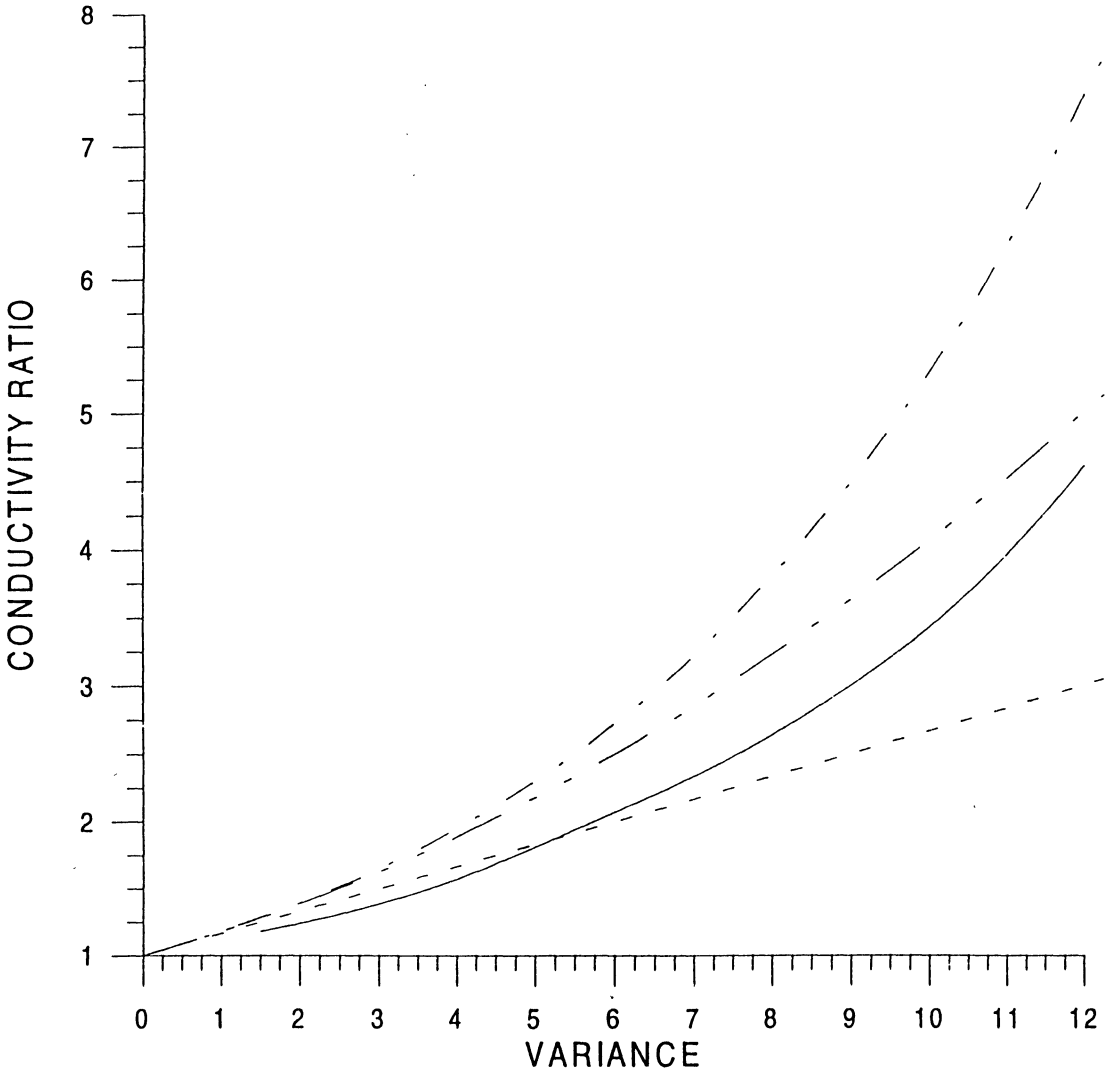

SYMBOLS:
—— Present simulations
----- Gutjahr et al (1978)
----- Matheron (1967)
—·—· Dagan (1993)

Figure 4-12. *Comparisons with theoretical estimates of* K_{eff} / K_G *versus variance of the conductivity logarithm. The solid line represents simulations with both fracture sizes.*

5 DISCUSSION

The general impression of the results from the testcases is that good agreement is obtained both with analytical solutions and relevant theoretical results. The method has however some limitations which are important to be aware of:

- For fractures that are thin in relation to the grid size, say $W/\Delta < 0.5$, the transmissivity may be represented with an error of a few percent. This has been clearly demonstrated in this report.

- The cell size Δ also sets a lower limit on the size of features that can be represented correctly in the grid. Obviously there is no possibility to take the orientation of a fracture, that is smaller than the cell size, into account. What is perhaps more important is that we cannot always resolve the space between two fractures. In Figure 5-1 this problem is illustrated. However, resolution problems are an inherent part of the discretization procedure and have to be accepted. If possible, one should estimate how sensitive the results are to the grid resolution by making runs with different grid sizes.

Regarding the accuracy it is found that a few percent of the transmissivity are lost when a fracture is represented as grid cell conductivities. It may then be a good idea to increase the transmissivity with a few percent to compensate for this loss. The correction should however only be one or two percent for fractures with $W/\Delta > 0.5$. The resolution problem, discussed above, increases the connectivity and hence the effective conductivity for realistic fracture networks. The two effects hence work in opposite directions and it is probably best not to compensate for the transmissivity loss.

The smallest fracture width used in the testcases with analytical solution is $W/\Delta = 0.125$. Small fractures are often best described as "a single opening" and the aperture is then less than, say, 1 mm. The fracture width from $W/\Delta = 0.125$ will always be orders of magnitude larger than this aperture. We also know that our method for representing fractures in the grid is sensitive to W/Δ. In Figure 5-1 some illustrations are shown. From these it is clear that a fracture will be represented almost the same way in the grid if $W/\Delta = 0.125$ or if the fracture is very thin. The recommendation is therefore: major fracture zones should preferably be given a width $> 0.5\Delta$, in order to keep the error in the calculated flow rates smaller than a few percent. No fracture should have a smaller width than about 0.1Δ, as the smallest width tested against the analytical solutions is 0.125Δ.

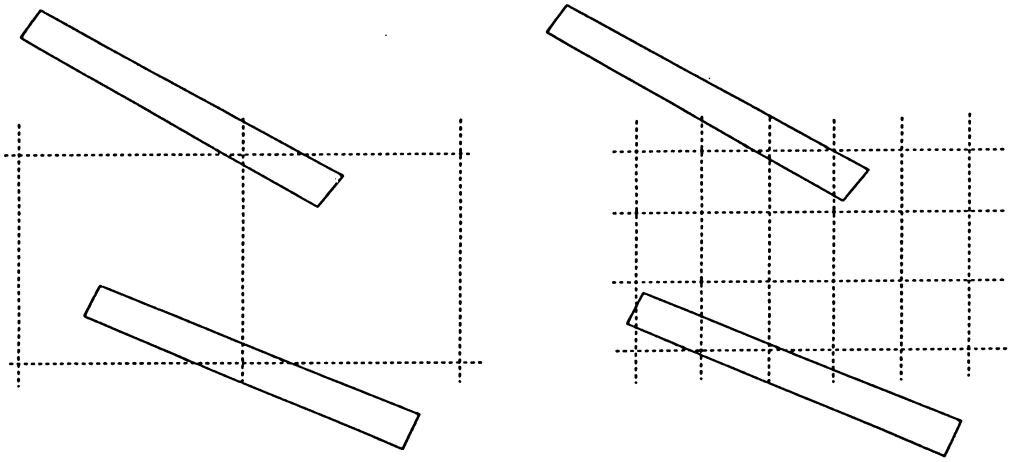

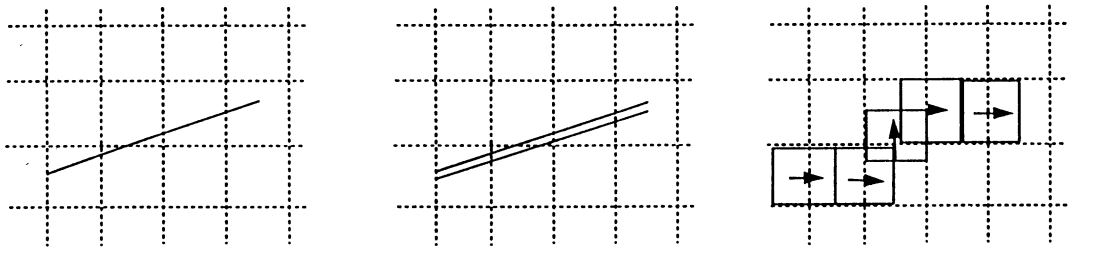

Figure 5-1. *Illustration of the resolution problem (top) and representation of thin fractures in the computational grid.*

A relevant topic for discussion is whether the testcases considered are adequate. One may, for example, criticise that all fractures, for the testcases with analytical solution, extended from the inlet to the outlet boundary. Further, for the testcases with one or several fractures in a 3D domain, the global pressure gradient was always in a coordinate direction. Does that limit the value of the tests? More testcases and combination of cases can always be suggested and may reveal new shortcomings of the suggested method. It is however believed that the crucial part in the evaluation of the method is to demonstrate the influence of the width of the fracture and the influence of the various angles the fracture makes with the coordinate directions. The testcase "a single fracture in a 3D domain" is thus perhaps the most important one. For this testcase, one may note that the direction of the global pressure gradient is at a varying angle to the fracture centre line, as the downstream position of the fracture changes. It is thus believed that the testcases considered are relevant, but it is also appreciated that new testcases may reveal new aspects of the suggested method.

6 SUMMARY AND CONCLUSION

The objective of this report is to establish how well the suggested method can represent a fracture network as grid cell conductivities. For this purpose five test cases have been carried out. The results from these can be summarised as:

- Comparisons with analytical solutions show that fractures that directly connect two opposite faces of the domain are represented with very high accuracy; if $W / \Delta > 0.5$, the error in the flow rate is $\leq 2\%$.

- A comparison with results from percolation theory shows that a connected fracture network is obtained at the right fracture density, i.e. the critical density or the percolation threshold. Fracture nets, at the percolation threshold, have been shown to result in connected flow channels.

- Theoretical results are available for how the conductivity for the whole domain is related to the properties of the cell conductivities. A qualitative agreement with these theories is demonstrated.

The general conclusion of the study is that the proposed method to represent fracture networks as grid cell conductivities is accurate enough for practical groundwater simulations.

7 ACKNOWLEDGEMENTS

The software package for generating the fracture network and the conductivity fields was written by Hans-Olof Kuylenstierna. His contribution has thus been of crucial importance to the project.

An earlier draft of this report was reviewed by Johan Holmén, Hans-Olof Kuylenstierna, Ingvar Rhén, Jan-Olof Selroos and Douglas Walker. Their constructive comments contributed to the improvement of the report.

8 REFERENCES

Bour O, Davy P, 1998. On the connectivity of three-dimensional fault networks. Water Resources Research, Vol. 34, No. 10, pp. 2611-2622, October 1998.

Charlaix E, Guyon E, River N, 1984. A criterion for percolation threshold in a random array of plates. Solid State Communications Vol. 50, No. 11, pp. 999-1002.

Dagan G, 1993. Higher-order correction of effective permability of heterogeneous isotropic formations of log-normal conductivity distribution. Trans. Porous Media, Vol. 12, pp. 279-290.

de Marsily G. and Renard Ph. 1997. Calculating equivalent permeability: a review. Advances in Water Resources. Vol. 20, Nos 5-6, pp. 253-278.

De Wit A, 1995. Correlation structure dependence of the effective permeability of heterogeneous porous media. Phys. Fluids 7 (11), November 1995.

Gutjahr A.L, Gelhar L.W, Bakr A.A & McMillan J.R, 1978. Stochastic analysis of spatial variability in subsurface flows 2: Evaluation and application. Water Resources Research, 14(5) (1978), pp. 953-959.

LaPointe P.R, Cladouhos T, Follin S, 1999. Calculation of displacements on fractures intersecting canisters induced by earthquakes: Aberg, Beberg and Ceberg examples. SKB Technical Report TR-99-03.

Matheron G, 1967. Eléments pour une Théorie des Milieux Poreux. Masson, Paris.

Rhén I (ed), Gustafson G., Stanfors R., Wikberg P. 1997. Äspö HRL – Geoscientific evaluation 1997/5. Models based on site characterization 1986-1995. SKB Technical Report TR-97-06.

Robinson P.C, 1984. Numerical calculations of critical densities for lines and planes. J.Phys. A:Math. Gen. 17 (1984), pp. 2823-2830.

Spalding D.B, 1981. "A general purpose computer program for multi-dimensional one- and two-phase flow". Math. Comp. Sim., 8, 267-276. See also: http://www.cham.co.uk.

Svensson U, 1999. A laboratory scale analysis of groundwater flow and salinity distribution in the Äspö area. SKB Technical Report TR-99-24.

APPENDIX A

DOCUMENTATION

CONDENSED DESCRIPTION OF GROUNDWATER FLOW MODEL.

Representation of fracture networks as grid cell conductivities	
Scope Comparisons with analytical solutions and theories	
Process description Conservation of mass and momentum (Darcy's law)	
CONCEPTS	**DATA**
Geometric framework and parameters	
Domain divided into computational cells to which conservation laws are applied.	Domain size: 100 x 100 x 100 m^3 Computational grid: 1 000 000 cells.
Material properties	
Hydraulic conductivities (K).	No field data is used.
Spatial assignment method	
Cell conductivities are calculated from a fracture network.	No field data is used.
Boundary conditions	
Zero flux or prescribed pressure.	No field data is used.
Numerical tool PHOENICS	
Output parameters Darcy velocities, pressure	

ISSN 1404-0344
CM Gruppen AB, Bromma, 1999